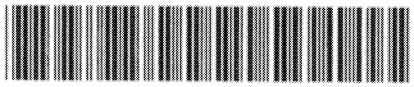

BB

MICHIGAN STATE
UNIVERSITY

National Superconducting Cyclotron Laboratory

PRODUCTION OF NEUTRONS WITH PROTONS OF 22, 30 AND 40 MeV

THOMAS M. AMOS, ROBERT R. DOERING, AARON GALONSKY, RAJ JOLLY, and MARY K. ZIGRANG

MSUCL-1266 JUNE 2003

Production of Neutrons with Protons of 22, 30 and 40 MeV[£]

Thomas M. Amos*, Robert R. Doering[§], Aaron Galonsky[†], Raj[1] Jolly[#], and Mary K. Zigrang*
NSCL/Cyclotron Laboratory and Department of Physics & Astronomy
Michigan State University, E. Lansing MI 48823, USA

Abstract

Stopping targets of C, Al, Cu, Ag, Ta and Pb were bombarded by protons of 22, 30 and 40 MeV and the resulting neutron energy spectra were measured down to 0.5 MeV at 30° intervals from 0° to 150°.

I. Introduction

When nuclei are bombarded with particles that have enough kinetic energy to produce neutrons, there is no practical way to prevent that production from occurring. For reasons of radiation safety, design of radiation shielding, and, possibly, background subtraction in radiatio experiments, it is useful to know both the energy and angle distributions of the produced neutrons when the nuclei are stopped in various materials. The same information is also needec if one wishes to produce a beam of neutrons for irradiation of materials or of certain cancers. Neutron production data have previously been obtained in experiments with energetic beams of nuclei of helium [1, 2] and of carbon [2].

In this paper we report on measurements of neutron production by protons at three energies—22, 30 and 40 MeV. There were six stopping materials—C, Al, Cu, Ag, Ta and Pb. For each proton energy and target material (only 22 and 30 MeV for Ag), spectra of the neutron were measured at six angles—0°, 30°, 60°, 90°, 120° and 150°, giving a total of 102 neutron spectra. Each spectrum was measured from the highest neutron energy, always less than 40 MeV, down to 0.5 MeV. The minimum energy of 0.5 MeV is low enough for determination of the essential features of the energy spectra.

II. Plan of the Experiment

The experiment was performed at the Michigan State University Cyclotron Laboratory, and the source of the protons was its K50 isochronous cyclotron.

The plan of the measurements was to detect and determine the energies of the neutrons emitted at each angle. To implement this plan we used: A) the time-of flight (*TOF*) method to determine neutron energy,) B) pulse-shape discrimination (*PSD*) to separate neutron-induced pulses from γ-ray-induced pulses, and C) flight paths of two different lengths to cover a large neutron energy range with good resolution.

[£]Submitted to *Nuclear Science and Engineering*

*Deceased

[§]Present address: Texas Instruments, P.O. Box 650311, MS 3730, Dallas, TX 75265

[†]E-mail: galonsky@nscl.msu.edu

[#]Present address: 48 Gainsborough Pl. , Newport News, VA 23608

A. *TOF.* A flight path between target and neutron detector was chosen. A signal from the detector, a scintillator/phototube, was used to start an electronic clock, a time-to-amplitude-converter (TAC) module. The stop signal was generated from alternate cycles of the cyclotron's rf. Using alternate cycles results in the length of time displayed being equal to two rf periods, in this experiment ~ 100 ns. A pulse of protons may still strike the target ~ every 50 ns and produce neutrons ~ every 50 ns. A neutron of a given energy may, for example, be detected and produce a TAC signal ~ 20 ns before the rf stop signal or, with equal statistical probability, ~ 70 ns, depending on which of two possible beam pulses produced the neutron. The result for an entire TOF spectrum is, except for a small pedestal section, a spectrum followed by its duplicate. Figure 1 shows a typical pair of such TOF spectra, the upper spectrum overwhelmingly of γ rays and the lower spectrum overwhelmingly of neutrons. (Separation into two sets of data is described below in Section IIB. PSD.) One of the striking things about this figure is the pair of spikes in each spectrum. These spikes result from the detection of *prompt* γ rays produced in the target. Because γ rays of all energies have the same speed, the spikes in the TOF spectrum corresponding to these prompt γ rays have width only because of instrumental resolution, and the figure tells us that the full-width-at-half-maximum (FWHM) is ~ 3.5 channels $\cong$ 0.4 ns. The conversion from channels-to-nanoseconds comes from the built-in calibration that the time between the two spikes equals one rf period, T_{rf}, 54 ns in Fig. 1.

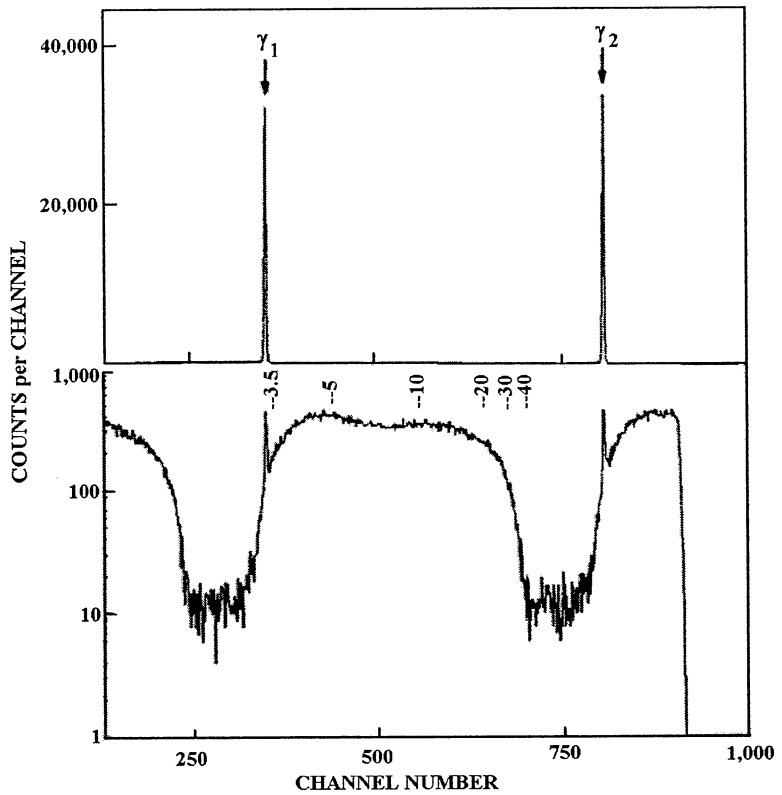

Fig. 1. Two TOF spectra at a forward angle produced with protons at 40 MeV. The upper spectrum is for γ rays, the lower spectrum for neutrons. Some neutron energies, from 3.5 to 40 MeV, are indicated.

The spikes also provide the calibration for determining neutron flight times through the simple equation

$$TOF_n = L/c + T_{rf}\frac{(Ch_{\gamma_2} - Ch_{\gamma_n})}{(Ch_{\gamma_2} - Ch_{\gamma_1})} \quad (1)$$

Once TOF_n is obtained from Eq. 1, neutron velocity and kinetic energy follow. Some neutron energies, from 3.5 to 40.0 MeV, obtained in this manner are indicated just above the neutron spectrum in the lower half of Fig. 1.

B. *PSD.* A problem with the neutron scintillation detector is that it is about equally sensitive to both neutrons and γ rays. Since both of these radiations are neutral particles, unaffected by magnetic fields and attenuated by matter only exponentially, there is generally no practical way to prevent the γ rays from reaching the detector without severely attenuating the neutron flux. However, with the liquid scintillator NE-213, a substance consisting of H and C atoms, it is possible by pulse-shape discrimination (PSD) to distinguish neutrons from γ rays and from cosmic-ray muons. In NE-213, most of the light is emitted with a time constant of a few ns, the remainder more slowly. The division between fast light and slow light depends upon the ionization density of the exciting particle. Lightly-ionizing particles, either electrons from Compton-scattered γ rays or relativistic muons, produce more of the fast fluorescence than do the more highly-ionizing protons scattered by neutrons or the α particles and protons resulting from breakup of C nuclei in NE-213. Hence, the shape of the pulse is different for the two categories of radiation [3-5], and PSD of the related photomultiplier signal can be used to identify the neutrons.

For this reason our scintillator was NE-213. We double-differentiated the phototube pulse and used the zero-crossing time to separate the two categories of pulses [6-9]. In this way we generated the separate neutron and γ-ray TOF spectra, as illustrated in the upper and lower parts of Fig. 1. The separation is not perfect, but one can see from Fig. 1 that the spikes of the γ rays appear in the lower spectrum, the neutron spectrum, attenuated by a factor of ~ 100.

Without PSD, spikes of *prompt* γ rays can be eliminated by a gate on TOF, with a consequent loss of that relatively small portion of the neutron TOF spectrum. In a neutron-production experiment, however, the detector sits in a sea of time-uncorrelated γ rays resulting mostly from inelastic scattering and capture of the very neutrons produced in the experiment, only a tiny fraction of which strike the detector. A TOF gate on these γ rays would leave no experiment. As we will see in Section IV, the high-energy neutrons are peaked strongly forward. The sea of γ rays is isotropic, with the consequence that the time-uncorrelated γ rays may be negligible in a spectrum like that of Fig. 1 but important in spectra at angles far from 0°.

C. *Neutron energy range vs. energy resolution.* For a given flight path, the lower limit of neutron energies which can be uniquely determined is limited by the pulse repetition rate of the beam, since at some energy faster neutrons will arrive at the detector at the same time as do slower neutrons produced by the preceding beam burst. This "overlap" causes the TOF spectrum to become confused, because one value on the time axis (Channel Number in Fig. 1) then corresponds to two or more energies. For example, the K50 cyclotron we used produces a beam of 40-MeV protons in bursts spaced 54 ns apart. To compress into 54 ns the entire neutron spectrum down to our goal of 0.5 MeV requires a flight path no longer than 50 cm. Unfortunately, we get poor energy resolution (see Section III) at the higher energies with such a small flight path—almost 6 MeV (FWHM) for neutrons at the highest-energy, 40 MeV.

By taking data at two flight paths—L = 150 cm and 50 cm—we were able to measure the entire spectrum with reasonable resolution. Since energy resolution from TOF scales as 1/L, the

resolution at 40 MeV is ~ 1.9 MeV with L = 150 cm. To defeat the overlap that occurs when L = 150 cm, we set a pulse-height threshold that rejected pulses from neutrons a bit below 3.5 MeV. (Figure 1 is a spectrum that was taken under these conditions.) For the energy range of 0.5-3.5 MeV the 50-cm flight path is sufficiently short to prevent overlap, and the energy resolution is 0.27 MeV at 3.5 MeV. The two spectra were joined together to give the complete energy spectrum.

A helpful side effect of dividing the data-taking into runs for neutrons of higher energy and lower energy was an accompanying division of detector pulse heights into larger and smaller. Because light production in NE-213 is non-linear with respect to energy deposited [10] (with low energies disfavored) the neutron energy range 40/0.5 = 80 converts into a pulse-height range of 400, far too great for the electronics to handle. With two energy ranges to make a complete spectrum the pulse-height range was reduced to a factor of ~ 20 in each run.

III. Experimental Details

A. *Target Chamber.* The proton beams were directed into a cylindrical target chamber 10 cm in diameter as illustrated in the side view of Fig. 2. Six targets plus a scintillator for viewing the beam spot were mounted on the target ladder. Remotely-controlled drive units, not shown, mounted on top were used for target selection and rotation. In operation, the target ladder was rotated by 45° from that shown in the figure. Each target was a cylinder 2.54 cm in diameter and of a thickness equal to the proton range in each material; there was a set of six targets for each proton bombarding energy. The targets were, therefore, stopping targets, but, for simplicity, excess target material was avoided in order to reduce scattering and reactions of the produced neutrons.

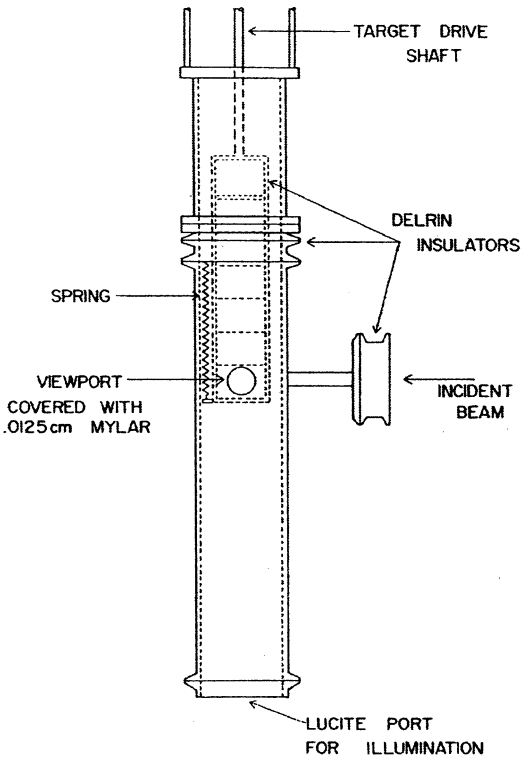

Fig. 2. Side view of target chamber. Six targets plus a scintillator, for viewing the beam spot, were mounted on the target ladder. Remotely-controlled drive units, not shown, mounted on top were used for target selection and rotation. In operation, the target ladder was rotated by 45° from that shown in the figure. The spring maintains electrical connection between the target ladder and the chamber.

B. *Faraday* Cup. In order to measure absolute production rates, it was necessary to determine the number of incident protons during each run. The integrated electrical charge brought into the target chamber provided these numbers. Most of the charge was produced within the bombarded target. To make the target chamber a good Faraday cup the targets and target holder were isolated electrically from the drive units by a DELRIN insulator and electrically connected to the chamber walls by a long flexible spring. The chamber itself was insulated from both the drive units and the adjoining beam pipe by DELRIN insulators. To reduce the possibility of incorrect charge collection due to escape of electrons from the chamber, the chamber included a long, narrow entrance.

C. *Detector.* The detector was NE-213 liquid scintillator encapsulated in a cylinder of glass with inside dimensions 4.44 cm diameter by 1.90 cm thickness. The cylinder was mounted on an RCA 8575 phototube. From the diameter, we get maximum angular acceptances of 1.7° and 5.1° for the 150-cm and 50-cm flight paths. As we will see, these values have negligible effects on the observed angular dependences of the neutron yields. The solid angles were .69 and 6.2 msr.

To make dead-time corrections negligible, the counting rate with this detector was kept below 10 kHz; this was accomplished by keeping the proton beam current within the limits of 0.1-10 nA.

D. *Energy Resolution.* Even if we could measure the time intervals with perfect accuracy, detector thickness ΔL limits the accuracy with which we can determine the time between the neutron's production in the target and its arrival at the detector because ΔL introduces an uncertainty in just where the detection occurs, i.e., in the value of the flight path L. The detector gives no information on the depth within the scintillator's 1.9-cm thickness at which the neutron interacted and produced a pulse of light. It would appear that TOF would be uncertain from this effect by a maximum value of $\Delta L / v$, v being the neutron's velocity, but when the index of refraction n of the scintillator is taken into account it can be seen, as follows, that this is an overestimate. Consider two neutrons of the same velocity. One neutron interacts and produces its light at the far end after time $\Delta L / v$. The other neutron produces its light at the front face, and that light reaches the far end after time $\Delta L \bullet n / c$. The difference between these two times is a better estimate of the effect of detector thickness:

$$\Delta L(\frac{1}{v} - \frac{1}{c/n}) \qquad (2)$$

Since neutron velocity in this experiment varied from 0.98 cm/ns at E = 0.5 MeV to 8.5 cm/ns at 40 MeV, and n = 1.5, the corresponding values of (2) range from 1.84 ns to 0.13 ns.

There is another, independent, source of time spread that would appear even if $\Delta L \rightarrow 0$. That source is mainly due to the length of the proton beam pulses and the spread of the transit time within the phototube. An approximate determination of that Δt can be obtained from the measured width of the TOF spike produced by the prompt γ rays, 0.4 ns FWHM in Fig. 1. For γ rays the detector thickness estimate of (2) is only 0.03 ns, which is negligible in comparison to 0.4 ns.

Since the two effects are independent, we combine them in quadrature to obtain

$$\Delta(TOF_n) = \{[\Delta L(\frac{1}{v} - \frac{1}{c/n})]^2 + (0.4)^2]\}^{1/2} \qquad (3)$$

At low energies the first term is the larger, at high energies the second term is the larger, and for our detector the two are equal at a neutron energy of 7.5 MeV. These comments are independent

of flight path. The relative error $\Delta(TOF_n)/TOF_n$ does depend on L, inversely. The relative error in neutron energy E is (non-relativistically) twice the relative error in TOF_n. For L =50 cm the energy error increases monotonically from 2.5% at 0.5 MeV to 7.8% at 3.5 MeV and for L = 150 cm from 2.6% at E = 3.5 MeV to 4.8 % at 40 MeV.

E. *Detector Efficiency*. For a neutron to be detected it must produce from the H and C in the scintillator a charged nucleus that will excite the scintillator molecules by electronic interactions. The possibilities are: a recoil proton from n-p scattering, a proton from the $^{12}C(n,p)^{12}B$ reaction, an α particle from the $^{12}C(n, \alpha)^{9}Be$ reaction or 3 α particles from breakup of ^{12}C. In a thickness of only 1.9 cm, with ~ 10^{23} H and C atoms/cm^2, the probability of any one of these interactions occurring is much less than 1. For example, the cross section for n-p scattering around 15 MeV ≈ 0.5 b, which means only 5% of the neutrons produce recoil protons. Since some of the protons will recoil with insufficient energy to produce the minimum light required to exceed the detection threshold, the n-p scattering contribution to *efficiency* will, in this case, be less than 5%. The reduction is particularly severe when the nucleus exciting an organic scintillator is an α particle or a low-energy proton because these highly-ionizing particles exhibit a saturation effect that yields less light per MeV of energy deposited than do more lightly-ionizing particles such as electrons [11]. For neutrons of energy < 20 MeV, light produced by α particles from the $^{12}C(n, \alpha)$ and $^{12}C(n, n3\alpha)$ reactions will be lost unless the threshold is quite low.

The energy dependence of the cross sections and of the light production in NE-213 [12] are known. These have been put together into the computer program TOTEFF [13] to generate energy-dependent efficiencies for each of the two thresholds used in our experiment. TOTEFF requires a pulse-height threshold and the pulse-height resolution at threshold. Calibrations of the detector for pulse height and resolution were done with the centroids and widths of the Compton edges of γ rays in the sources listed in Table I. For ^{57}Co we also saw, and used, the photopeak.

Table I.
Sources used for detector calibration.

Source	E_γ(keV)	E_{Comp}(keV)
^{57}Co	123.5	41
^{203}Hg	279	146
^{22}Na	511	341
^{137}Cs	662	478
^{22}Na	1280	1067
^{60}Co	1330	1116
^{208}Tl	2640	2380
$^{12}C^*$	4440	4190

The results are shown in Fig. 3. The thresholds for the two curves are 0.060 and 0.85 MeVee; 1 MeVee is the light produced by an electron of energy 1.0 MeV. The corresponding resolutions are 18% and 6%. In terms of neutron energy, *via* recoil protons, both thresholds are at much higher energies — ~ 0.5 MeV and ~ 3 MeV. The factor of 6 between these two neutron energies corresponds to a factor of 24 in light output. These numbers illustrate the light saturation effect discussed above. The peak efficiencies are ~18% and 6%, but neither efficiency curve drops sharply to zero because of the finite detector resolution. Especially in the lower curve we see

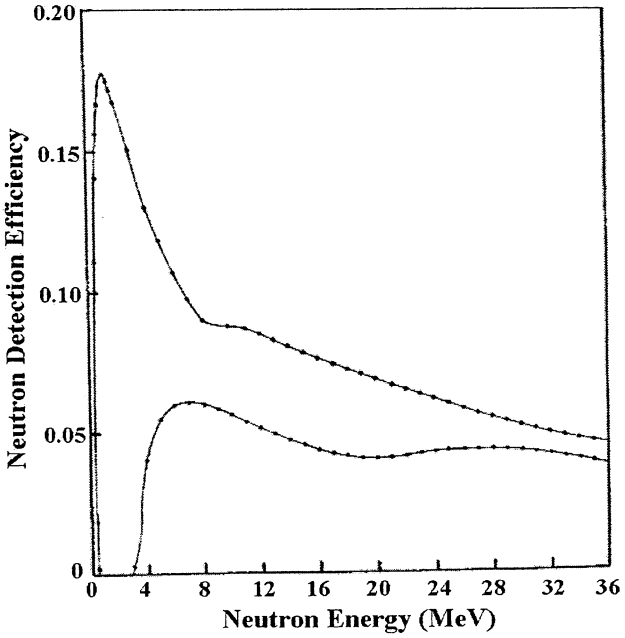

Fig. 3. Calculated energy dependence of detector efficiency for two different pulse-height thresholds, 0.06 MeVee for the upper curve and 0.85 MeVee for the lower curve. The corresponding resolutions at threshold are 18% and 6%.

both the decrease of efficiency as the cross section for n-p scattering decreases with energy and the increase of efficiency as α-particle production rises from its nuclear thresholds. We took care with pulse-height calibration because, as Fig. 3 shows, efficiency values very close to threshold are sensitive to that calibration as efficiency rises from zero to a peak in a small energy interval.

IV. Results

A. *Corrections, Errors, Basic Spectra.* Before the data were plotted corrections were made for deadtime of the electronics and for interactions of the neutrons within the stopping targets. Depending on beam intensity and neutron yield, the deadtime corrections were in the range of 5% to 15%. Corrections for neutron interactions were more complex but the results were of no greater magnitude. The calculations involved the detailed geometry of neutrons moving through the target. With the target at affixed angle of 45° with respect to the beam, the neutron path length through the target varied with angle in the manner shown in Fig. 4. Both the elastic and inelastic cross sections [14] were required, as were angular distributions [15]. Offsetting reactions and scattering that reduced the number of neutrons reaching the detector was inscattering from neighboring parts of the target that increased the

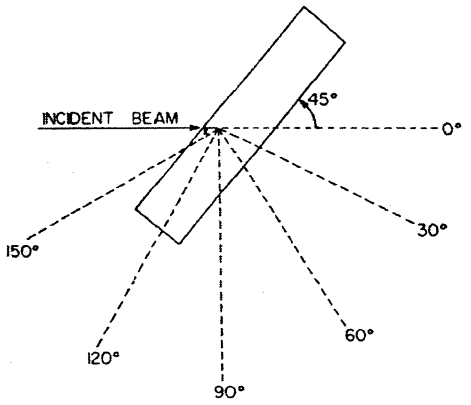

Fig. 4. Neutron paths through target for the six detection angles.

number. The net result depended on target, angle, and neutron energy but was generally within ~ ±10%.

The error in the latter corrections is estimated to be ±5%, but a larger error is in the neutron detection efficiency, which has been estimated [13] to be ±10%. Finally, when the data for the two ranges of energy, 0.5 to 3.5 MeV and ≥ 3.5 MeV, were joined in the region around 3.5 MeV, the typical mismatch was ~ ±10%. Combining these errors in quadrature gives a final error of ~ ±15%.

Figures 5-10 give the main results of this paper—graphs of absolute neutron energy spectra every 30° from 0° to 150°.

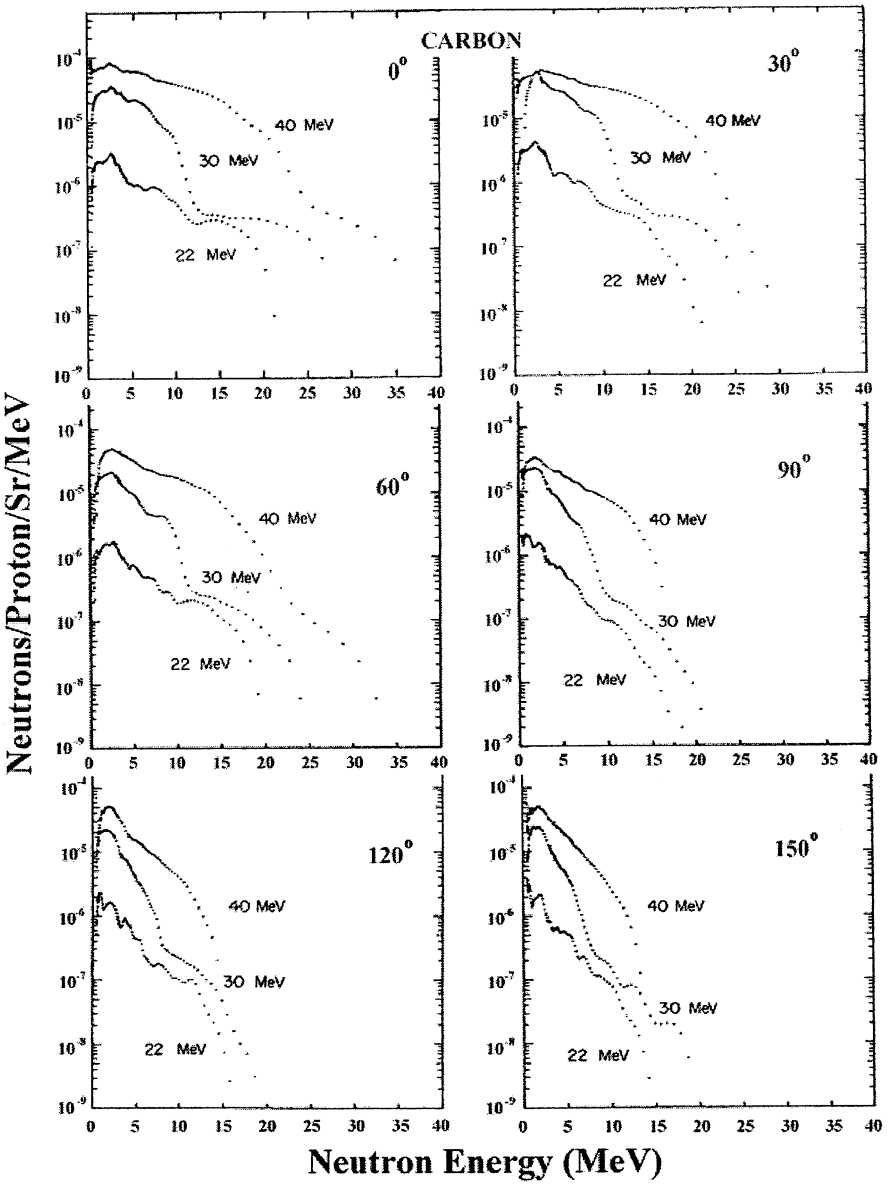

Fig. 5. Neutron yield spectra at 0°, 30°, 60°, 90°, 120° and 150° from stopping C targets bombarded by protons at energies of 22, 30 and 40 MeV.

B. *Features of the Basic Spectra.* Clearly, the regularities seen in the spectra from the Al, Cu, Ag, Ta and Pb targets are not in the spectra from the C target. Two properties that set aside the C target from the others are the relatively small number of nucleons, only 12 or 13, in C nuclei and the relatively high threshold for neutron production in ^{12}C, 19.6 MeV. The latter means that the 1.1% of ^{13}C in C is the entire source of the higher-energy neutrons. Especially in the forward-angle C spectra produced by protons of energy E_p = 30 MeV, one can see a rapid decrease in yield begin at E_p ~ 10 MeV.

The small number of nucleons in C nuclei means that (p,n) transitions to individual states can be important enough to override the smoothing effect of the target being thick. Only in the 40-MeV spectra do we see a smoothness comparable to that of the spectra of the heavier targets.

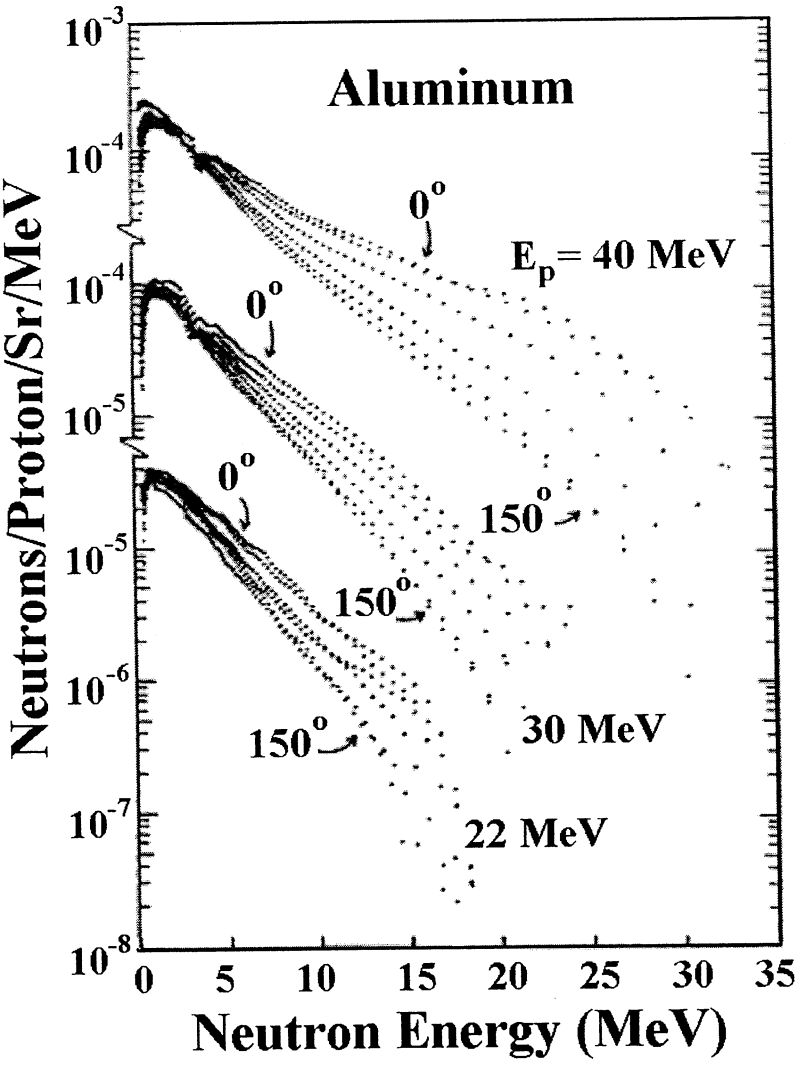

Fig. 6. Neutron yield spectra from stopping Al targets bombarded by protons at energies of 22, 30 and 40 MeV. Each energy group has spectra at 0°, 30°, 60°, 90°, 120° and 150°. Between the spectra labelec 0° and 150° are the other four spectra in monotonically descending order.

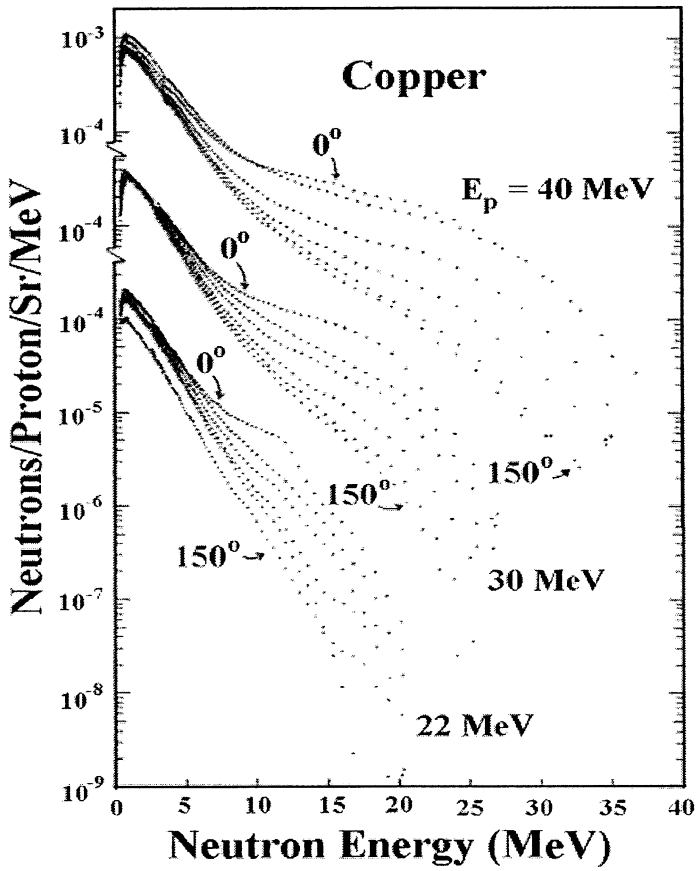

Fig. 7. Target nucleus is Cu. See Fig. 6 caption.

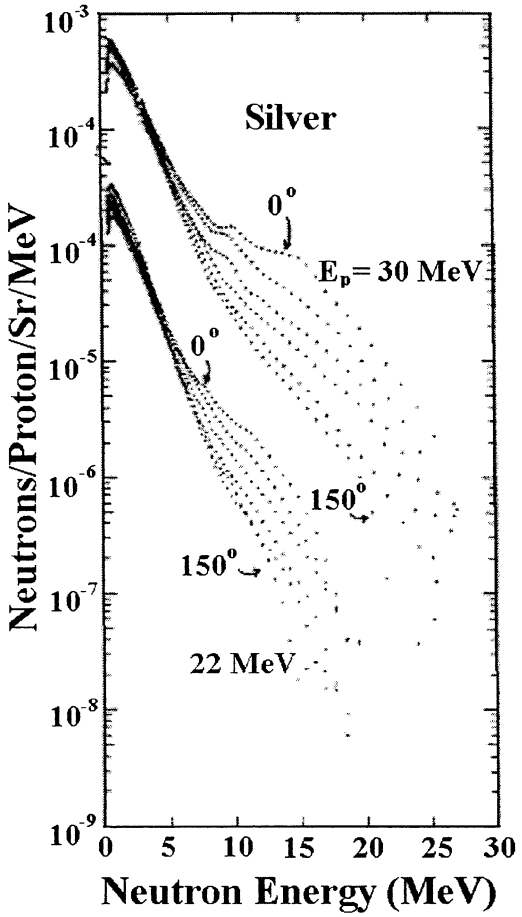

Fig. 8. Target nucleus is Ag. See Fig. 6 caption.

The spectra of those heavier targets have two components—a component that is almost isotropic at the lower energies (especially for the three heaviest targets) and a component whose angular distribution is forward-peaked at the higher energies. Although not in color, the groupings of the spectra have a beauty reminiscent of the peacock. The nuclear reaction mechanisms responsible for the two components are well understood as arising from compound nucleus [16] formation and from pre-equilibrium reactions [17]. Compound nucleus reactions are dominant at proton bombarding energies of the order of nucleon binding energies, typically somewhat less than 10 MeV, whereas pre-equilibrium reactions are significant at energies greater than ~ 20 MeV. Emission from a compound nucleus is isotropic and consists of low-energy particles; neutrons are the favored emission particle because they have no Coulomb barrier to penetrate. Pre-equilibrium emission is forward peaked and consists of high-energy particles. An expanded discussion of these two models as well as more details of the experiment are in Ref. [18].

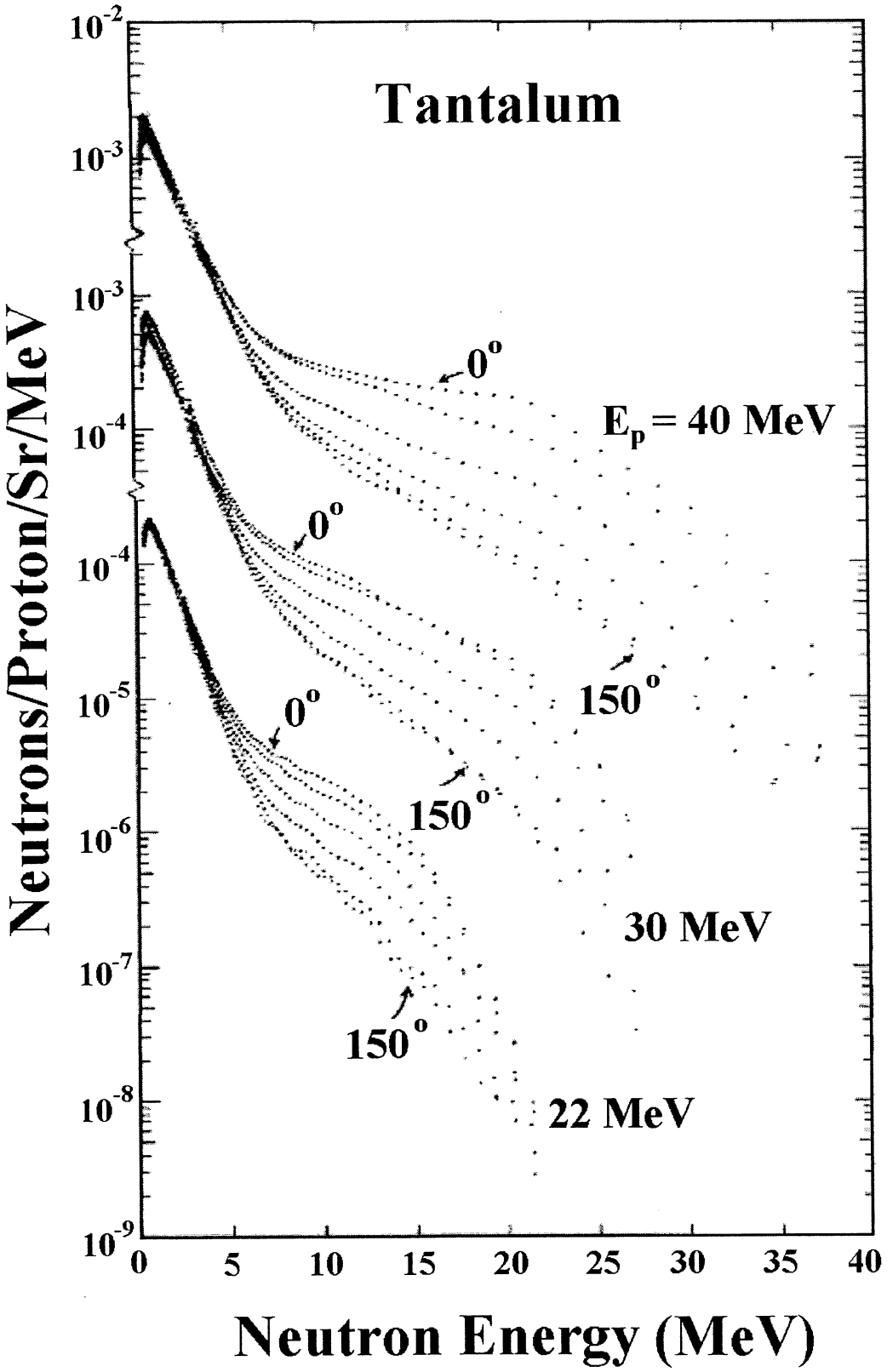

Fig. 9. Target nucleus is Ta. See Fig. 6 caption.

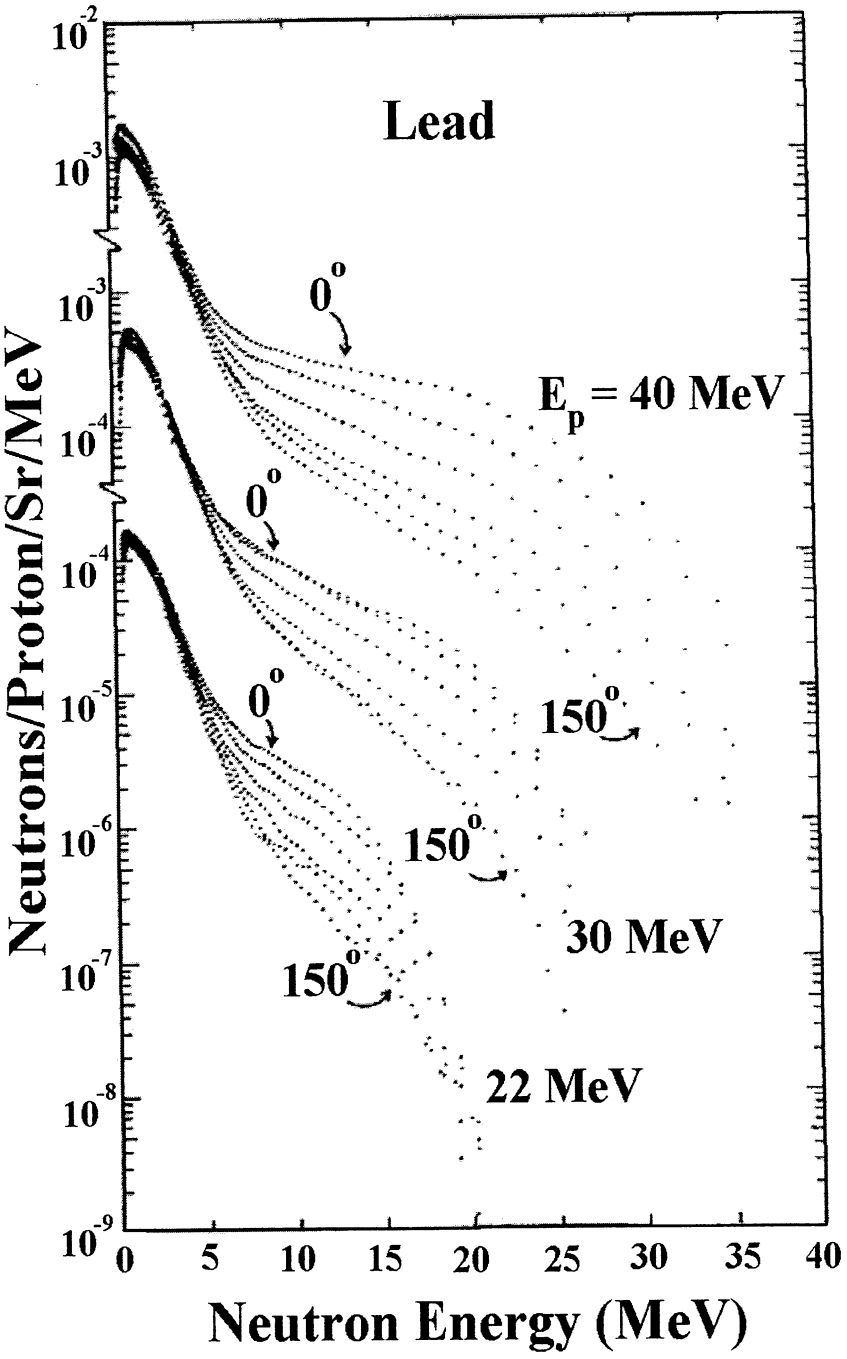

Fig. 10. Target nucleus is Pb. See Fig. 6 caption.

C. *Angular Distributions*. The basic spectra in Figs. 5-10 were integrated over energy to obtain the angular distributions shown in Fig. 11. Except for the C target, there is a similarity in the

shapes of the angular distributions—flat, except for a slight forward peaking—at all three proton bombarding energies. For each of those five targets the absolute values increase by a factor of 2-3 when the proton energy increases from 22 to 30 MeV, and by another factor of 2-3 from 30 to 40 MeV. And those absolute values are almost the same for the four heaviest targets.

With the sixth target, C, the forward peaking is larger, and the absolute values are lower, especially for proton energy equal to 22 MeV. At this energy the burden of neutron production falls heavily on the 1.1% of ^{13}C in the target. As noted in the caption to Fig. 11, the vertical scale for the C angular distributions is a factor-of-ten smaller than for the other targets.

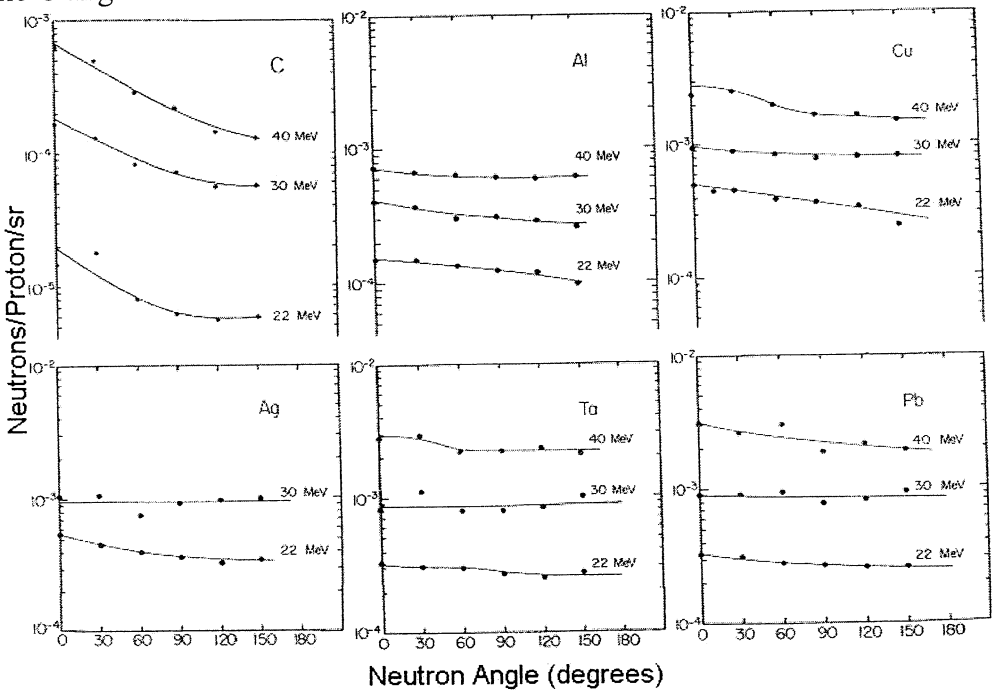

Fig. 11. Neutron angular distributions with the six targets and three proton energies.

D. *Neutron Total Yields.* Finally, we integrated the angular distributions in Fig. 11 to obtain the total neutron yields shown in Fig. 12. As could be anticipated from the angular distributions in Fig. 11, the yields with the C target are the lowest of the six, those with the Al target are next, and the yield with Cu, Ag, Ta and Pb are the largest and are almost the same as each other. Included in this figure are measurements of thick-target yields obtained by Tai *et al.* at 18 and 32 MeV [19]. The Tai experiment was performed by neutron activation of a $MnSO_3$ bath. When the great difference between their technique and ours is considered, the agreement of the results of the two experiments is excellent with regard to both the absolute magnitudes of the total yields and the behavior of these yields as a function of bombarding energy.

Stopping a proton beam of energy below 40 MeV in a block of carbon is clearly a way to minimize neutron production, especially if the carbon was depleted in ^{13}C.

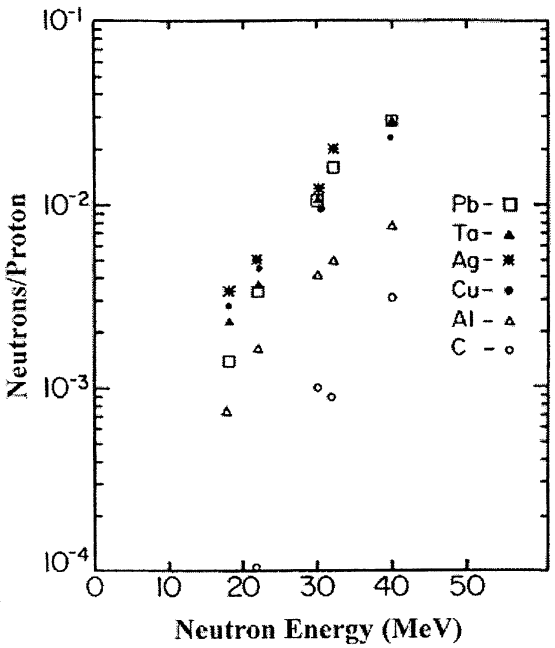

Fig. 12. Neutron yields integrated over both neutron energy and angle with the six targets and three proton bombarding energies. The data at 18 and 32 MeV were taken from Ref. 19.

Acknowledgement

Support of the U.S. NSF under Grant No. PHY-01-10253 is gratefully acknowledged.

References

[1] R.A. Cecil, B.D. Anderson, A.R. Baldwin, R. Madey, A. Galonsky, P. Miller, L. Young, and F.M. Waterman, Phys. Rev. C **21**, 2471 (1980).

[2] L. Heilbronn, R.S. Cary, M. Cronqvist, F. Deak, K. Frankel, A. Galonsky, K. Holabird, A. Horvath, A. Kiss, J. Kruse, R.M. Ronningen, H. Schelin, Z. Seres, C.E. Stronach, J. Wang, P. Zecher, and C. B. Zeitlin, Nucl. Sci. and Eng. **132**, 1 (1999).

[3] R. Owen, IEEE Trans. Nucl. Sci. NS-5 (1958) 198.

[4] J.B. Birks, The theory and Practice of Scintillation Counting, Pergamon Press, Oxford, 1964, pp. 219-227 and 392-394.

[5] P. Sjolin, Nucl. Instr. Meth. **37**, 45 (1965).

[6] M. Rousch, M. Wilson and W. Hornyak, Nucl. Instr. & Meth. **31**, 112 (1964).

[7] P. Sperr, H.Spieler, M.R. Maier, and D. Evers, Nucl. Instr. & Meth. **116**, 55 (1974).

[8] R. St. Onge, Aaron Galonsky, R.K. Jolly, and T.M. Amos, Nucl. Instr. & Meth. **126**, 391 (1975).

[9] G. Randers-Pehrson, R. W. Finlay and D. E. Carter; Nucl. Instr. & Meth. **215**, 433 (1983).

[10] V. Verbinski, W. Burrus, T. Love, W. Zobel, N. Hill and R. Textor, Nucl. Instr. & Meth. **65**, 8 (1968).

[11] J.B. Birks, The theory and Practice of Scintillation Counting, Pergamon Press, Oxford, 1964, pp. 219-227 and 392-394.

[12] V. Verbinski, ... NIM

[13] R. Kurz, University of California Report UCRL-11339, 1964 (unpublished).

[14] D. Hughes and R. Schwartz, "Neutron Cross Sections," **BNL 325**, U.S. Government Printing Office (1958).

[15] D. Garber, L. Stromberg, M. Goldberg, D. Culleo and V. May, "Angular Distributions in Neutron-Induced Reactions," Vol. II, **BNL 400** (1970).

[16] N. Bohr, Nature **137**, 344 (1936).

[17] M. Blann and A. Mignerey, Nucl. Phys. **A186**, 245 (1972].

[18] Thomas M. Amos, Ph.D. thesis, Michigan State University (1972).

[19] Y.-K. Tai, G.P. Milburn, S.N. Kaplan and B.J. Moyer, Phys. Rev. **109**, 2086 (1957).